13th World Conference on Earthquake Engineering
Vancouver, B.C., Canada
August 1-6, 2004
Paper No. 381

DYNAMIC TEST AND ANALYSIS OF AN ECCENTRIC REINFORCED CONCRETE FRAME TO COLLAPSE

Yousok KIM[1], Toshimi KABEYASAWA[2]

SUMMARY

A shaking table test was conducted to investigate the torsional response characteristics of a reinforced concrete frame with asymmetric plan consisting of a shear wall and independent columns, and the shear collapse mechanism of the columns designed in accordance to the 1970s Japanese design practice resulting vulnerable to shear failures. The specimen was subjected to five different earthquake base motions scaled appropriately so that the response will be from elastic to inelastic, and finally to collapse. The observed displacement responses, which were considerably different between the stiff and flexible frame, were presented and the torsional response ratio magnified from linear to nonlinear range were also described. In the final run, the process of shear strength deterioration of the independent columns was illustrated with observed responses such as forces, displacements and transverse reinforcement strain, and finally showed shear failure followed by axial load collapse.

A macro model for RC column was proposed to simulate the experimental results, which is based on the plane strain-plane stress state and smeared rotating crack approach. The salient features of the proposed model are the capability of considering strength deteriorating effect resulting from the softening behavior in concrete constitutive law and the bending, shear and axial force interaction formulated from the stress resultants. The nonlinear analysis algorithm using two iterative schemes is illustrated, both of which are continued till the force and the stress equilibrium condition is satisfied.

Finally, the analysis result of the proposed model was verified through comparison with the observed response, by which the strength softening effect on the shear collapse process was clarified. The limitation of the model and the future research needs are also discussed.

INTRODUCTION

Among the characteristics of structures that have suffered severe damage or collapse during past earthquakes, the items to be investigated in this experimental and analytical study are as follows: (1) the

[1] Graduate Student, Department of Architecture, Graduate School of Engineering, The University of Tokyo, Tokyo, Japan. Email:yskim@eri.u-tokyo.ac.jp
[2] Professor, Earthquake Research Institute, The University of Tokyo, Tokyo, Japan. Email:kabe@eri.u-tokyo.ac.jp

lack of shear strength in RC columns designed following 1970's Japanese reinforcement detail practice, which lead to shear failure and the loss of axial load carrying capacity, (2) asymmetric plan system composed of independent column frame and wall frame, which induce considerable stiffness and strength eccentricity and hence concentrate damage on weak frame. The objectives of this experimental study, therefore, are to understand the collapse process of columns with poor shear capacity and to assess the influence of stiffness and strength eccentricities on elastic and inelastic earthquake responses.

Analytical study is performed for the first objective of this study. Several nonlinear analytical models have been proposed for reinforced concrete column, taking into account not only complex interaction effects but also strength degradation. These models can be categorized into two fields in terms of the hysteretic model used for representing the deteriorating characteristics, although hybrid model combining two hysteretic models was also proposed.

One is the member hysteretic model based on the force-deformation relation constructed from the member-level experimental studies, which usually adopted in a lumped plasticity model. This analytical approach is simple and economical but the way of defining strength deterioration and coupling effect between bending and shear is formulated using empirical formulation that entirely depend on the experimental data rather than based on the closed form equation. Therefore, the extensive experimental data are needed for improving the accuracy and reliability of the model.

The other one is material model (i.e. concrete and reinforcement) that is formulated in terms of stress-strain relation. These models are generally implemented in the finite element model, which are capable of representing the detailed local behavior and the more accurate description of inelastic behavior compared to the member hysteretic model. In addition, bending, shear and axial force interaction can be incorporated in an explicit way based on the stress-strain relation, and strength softening effect also formulated in a relatively rational manner despite this is also based on the experimental results. It is well known fact, however, that finite element model based on the material constitutive models requires the refined mesh division for the accurate estimation of the inelastic behavior in RC structures and, therefore, is not suitable for the nonlinear frame analysis in terms of the computation efforts.

This paper, compromising between accuracy and economical requirement in analytical model, proposes the reinforced concrete column model composed of only three elements representing two hinge regions and central part between them, the inelastic properties of which are based on the two-dimensional material constitutive models..

TEST SPECIMEN AND EXPERIMENTAL SETUP

Specimen

A one-third scale reinforced concrete specimen was tested on the shake table, which comprises a wall and a column frame in the first story and wall frames only in the second story as shown in Figure 1. Asymmetric plan in the first floor generate considerable stiffness and strength eccentricity amount up to 0.24 and 0.25, respectively. The stiffness eccentricity in the first story is given by:

$$R_{e_{kx}} = \frac{e_{kx}}{\sqrt{a^2 + b^2}}, \qquad e_{kx} = \frac{\sum {}_i k_x \cdot {}_i l_y}{\sum {}_i k_x} \tag{1}$$

Where e_{kx} is the distance between center of stiffness and mass, ${}_i l_y$ is the distance of each frame from center of mass, a and b are the dimension of plan in longitudinal and transverse direction, ${}_i k_x$ is stiffness

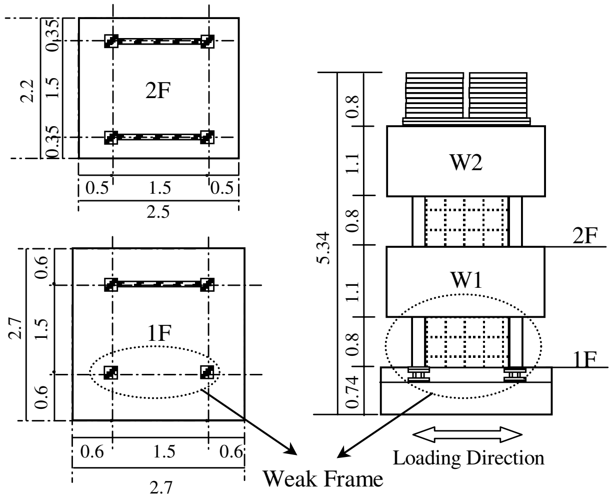

(a) plan (b) elevation

Figure 1 : Test Specimen (unit : m)

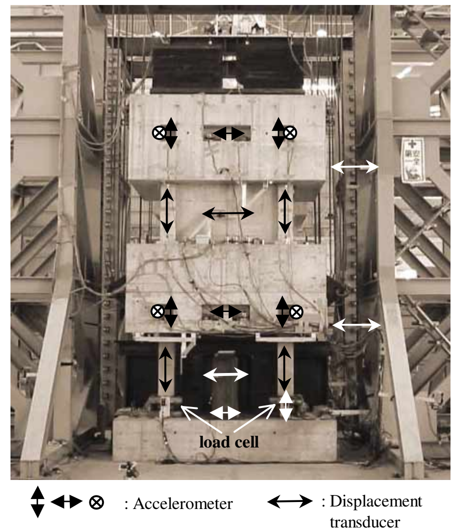

Figure 2: Experimental setup and instrumentation

of i frame in loading direction, x, which was calculated from pushover analysis in elastic range, and $\sum_i k_x$ is the sum of stiffness of all frames in loading direction.

Each frame's strength ${}_i q_x$ was calculated using material properties from concrete cylinder test and tensile test of sample bars, which can be found in Kim [1], and then used to calculate the strength eccentricity following Equation (2), where e_{qx} is the eccentric capacity of the frames to the mass and C_B is the base shear coefficient.

$$R_{e_{qx}} = \frac{e_{qx}}{\sqrt{a^2+b^2}}, \qquad e_{qx} = \frac{\sum_i q_x \cdot {}_i l_y}{\sum_i q_x} \cdot C_B \tag{2}$$

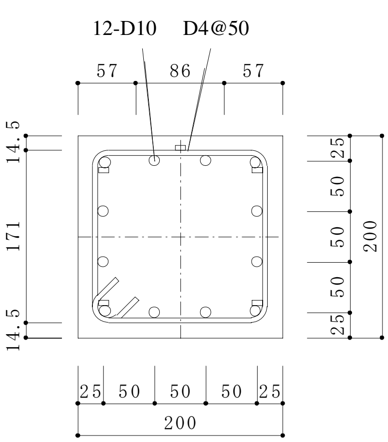

Figure 3 : Column detail

Total height of specimen is 5340mm, which is the summation of base (500mm), load cell (240mm), the first story (800mm), W1 (1100mm), the second story (800mm), W2 (1100mm) and steel plates (800mm) (Figure 1). Two concrete masses, W1 and W2 (284.6 KN), and steel plates (148.3 KN) on the specimen produced axial load stress, 0.15 $A_g f_c$ ($f_c = 18MPa$)) in the first story column, which correspond to that of six-story building. The first story independent columns were designed in accordance to 1970's Japanese reinforcement detail practice as shown in Figure 3, which are vulnerable to shear failure after flexural yielding.

Base Motion Input Plan and Instrumentation

The specimen was subjected to the series of base motion with selected five levels as shown in Table 1. The levels of the base motions were determined on the basis of preliminary analysis results, from which the RC specimen was expected to collapse at the stage 5 (CHI50). The duration time of the base motions was scaled by $1/\sqrt{3}$ to satisfy the similitude law. The axial stresses and the shear coefficients corresponded approximately to those of the proto-type six-story building by imposing the additional mass (steel plates) on the specimen. Before and after the input of base motions, a white noise input with low acceleration level was run to observe the change of the natural frequency of the damaged specimens.

The responses of the specimens, such as accelerations, displacements, strains in steel bars and shear and axial forces in the first story columns, were recorded in 1000Hz sampling rate with accelerometers (22 channels), displacement transducers (20 channels), electrical resistance strain gages (36 channels) and load cells (4 channels), respectively. The experimental setup and location of measuring instruments are shown in Figure 2.

Table 1: Base motion input plan

Earthquake data	Maximum target velocity	Ratio to the prototype	Maximum acceleration of prototype	Maximum velocity of prototype	Maximum acceleration input to specimen	Maximum velocity input to specimen
	(kine)		(gal)	(kine)	(gal)	(kine)
TOH	12.5	0.3	258.2	40.9	77.5	7.2
TOH	25	0.6	258.2	40.9	155	14.4
ELC	37.5	1.1	341.7	34.8	375.9	21.7
JMA	50	0.6	820.6	85.4	492.4	28.9
CHI	50	0.7	884.4	70.6	619	28.3

-TOH : Miyagi-ken Oki earthquake recorded at Tohoku university in 1978,
-ELC : Imperial Valley earthquake recorded at El centro in 1940
-JMA : Hyogo-Ken Nambu earthquake recorded at Japan Meteorological Agency in 1995
-CHI : Chile earthquake in 1985

TEST RESULTS

Damage Process of Specimen

The damage identification of the specimens was estimated with three methods, which were observation of cracks generated in specimen, the number of yielded strain gage attached to reinforcing bars and the change of natural frequency calculated from system identification method. The details of the results are discussed in Kim [1].

Lateral and Torsional Responses

Figure 4(a) shows the horizontal displacement responses of the wall and the column side during ELC37.5, which were measured from the displacement transducer instrumented between the base and the bottom of W1. The horizontal displacement response of the column side was much larger than that of the wall side, which resulted from the torsional response of the specimen with considerable eccentricity. The similar responses were observed in the other input stages although not presented here.

The extent of the torsional response in elastic and inelastic range was evaluated by the index r, indicating the relation between lateral displacement of center and rotation angle (Figure 4(b)). For instance, the value of r becomes zero in case of pure torsional mode and infinite in case of parallel translation mode. Namely, the torsional responses become dominant as the value of r decreases. As shown in Figures 4(c), the index r becomes small with the specimen damaged by increased load level, which suggests that the torsional response became more dominant in inelastic range rather than in elastic. These results may be explained in terms of the fact that strength eccentricity of this specimen, governing the characteristic of torsional response in inelastic range, is so high that the wall side was not yielded in spite of yielding of columns.

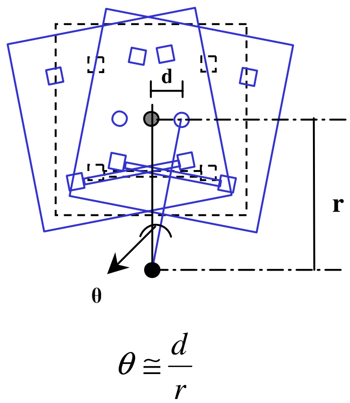

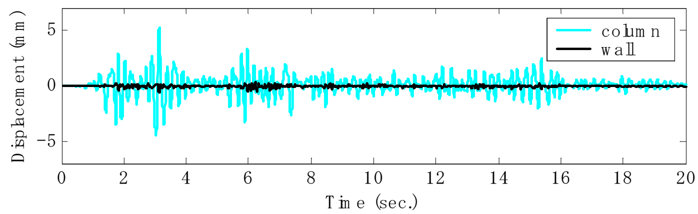

(a) Displacement response

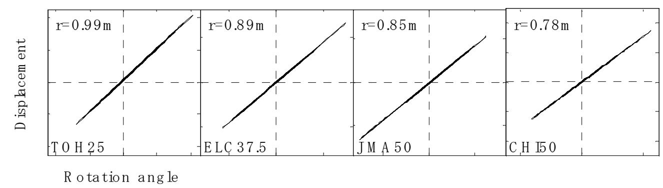

(b) Definition of r

(c) Relation between lateral displacement and rotation angle

Figure 4 : Torsional response

Shear Force Distribution

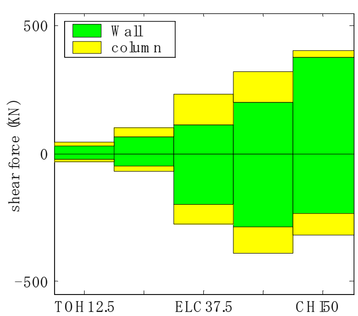

(a) column vs. wall

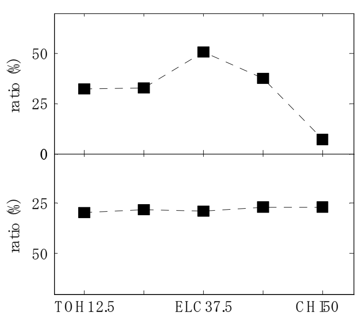

(b) ratio of column to base

Figure 5 : Shear force distribution carried by columns and wall

The base shear force was computed summing up the external forces calculated by multiplying masses of W1 and W2 to the acceleration record of them. Subsequently, shear forces carried by wall was calculated by subtracting shear forces, recorded at the load cells instrumented at the base of the independent columns, from base shear force. Figure 5(a) illustrates the shear forces carried by the columns and the wall in the 1st story, and the ratio of the column shear force to the base one is shown in Figure 5(b). Note that all the shear forces presented in Figure.5 are the values at the time when the base shear force attained the peak in both directions. From these figures, it is seen that the shear force carried by the columns is relatively smaller than that of wall and degrade gradually with increasing inelasticity.

Horizontal Displacement vs. Shear Force

The hysteretic relations between the horizontal displacement and the shear force of the two independent columns are presented in Figure 6. The solid and dotted lines are calculated shear strength (112.9KN) and shear at calculated flexural strength (125.5KN) of two columns, respectively.

In TOH12.5 and TOH25, the relation between two responses is almost linearly elastic, and as the load level increases, the stiffness degrades and the lateral drift becomes larger. The maximum shear forces were attained during JMA50, which was almost the same as that of the calculated strength. During the response to CHI50 input, the stiffness and strength degradations of the specimen became rapidly significant under reversed cyclic loadings and resulted in collapse when the elapsed time was around 20 sec.

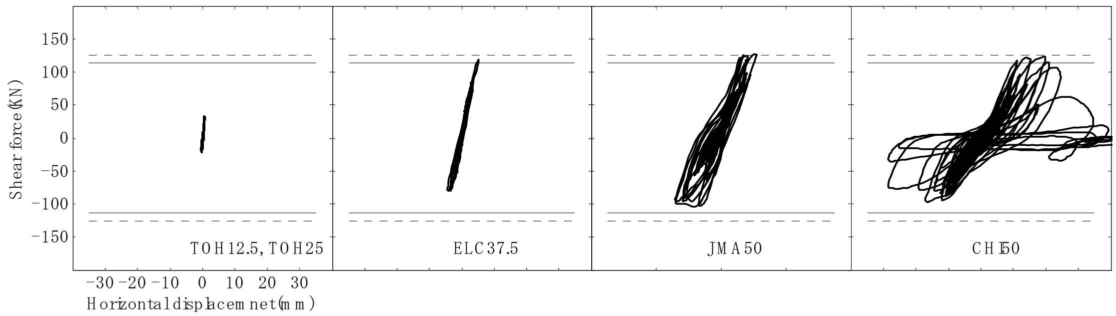

Figure 6: Shear force and displacement relation

Collapse Process of Columns

To investigate the process of RC column failure, the time-history responses and their relations observed for 10 seconds are illustrated in Figure. 7, which are from 12 sec. to 22 sec. after CHI50 base motion was run. The strain history of the transverse reinforcement shown in Figure.7 was measured at the mid-height of the column. Two reference times were selected to divide the responses into three parts. At first reference time, 16.7 sec, marked with black triangles, the large peak in shear force was recorded and then both the stiffness and strength degraded considerably and lateral reinforcement bar started to expand.

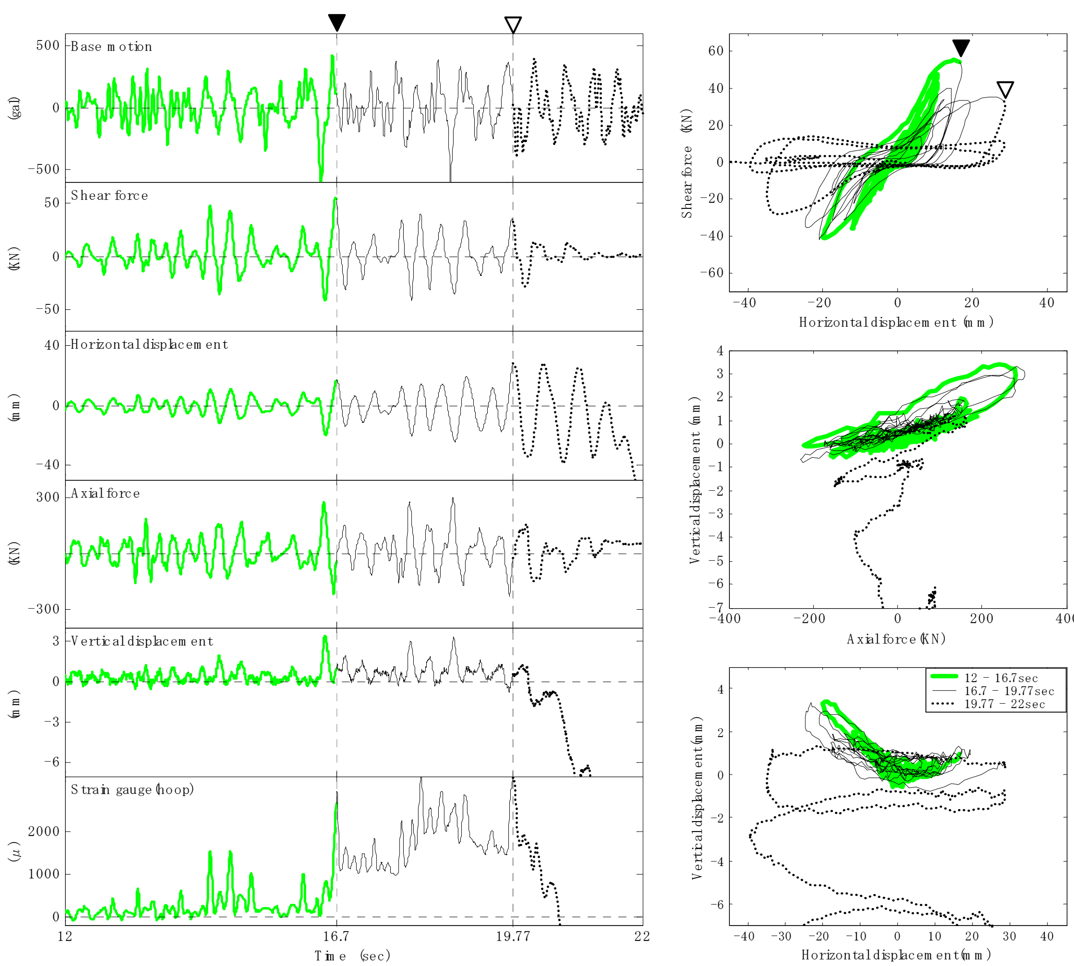

Figure 7 : Responses of east column in RC specimen during CHI50

Subsequently, at 19.77sec marked with white triangle, larger lateral drift was developed comparing to the previous one and lateral stiffness and strength was lost entirely, and finally, the loss of axial load-carrying capacity led the specimen to collapse.

From these figures, the process and the cause of the column axial failure may be interpreted as follow: the column response at the first peak induced the critical cracking associated with the yielding of the hoop, which caused the residual hoop strains and the shear strength decay. The second peak drift exceeded the previous maximum. Here, the hoop might be fractured since the residual strain fall down, and the loss of the interface shear transfer along the shear cracking might cause the fatal loss of the axial capacity. It should be noted that the inelastic strain of the hoop was accumulated with cyclic load reversals in the second time region and this could be the main cause of the shear and axial failure of the column.

ELEMENT FORMULATION

A column member in frame analysis is generally idealized by one line element with two-end nodes as shown in Figure 8(a). In the proposed model, however, the element is divided into three line elements by inserting two internal nodes (3,4) located at αL_0 from two external nodes (1,2) (Figure 8(b)), which represent the boundaries of the plastic hinge regions. Furthermore, as shown in Figure 8(c), each line element is transformed to plate element with 4 nodes. The procedure of deriving member stiffness matrix is described below.

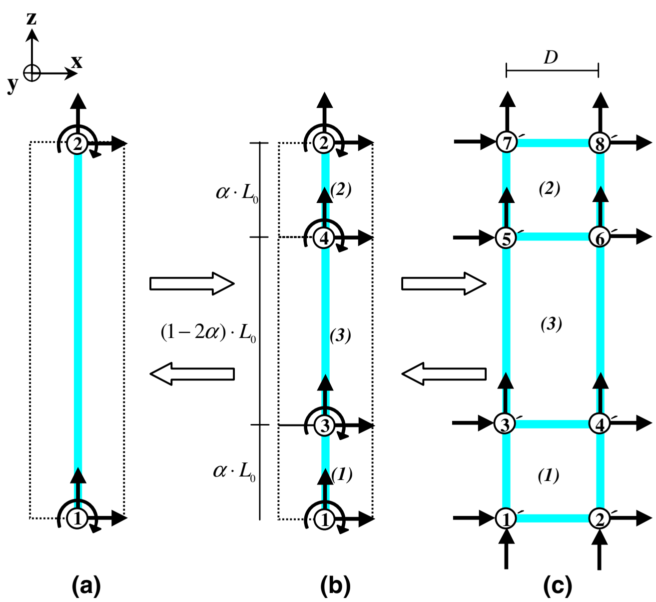

Figure 8 : Proposed column model

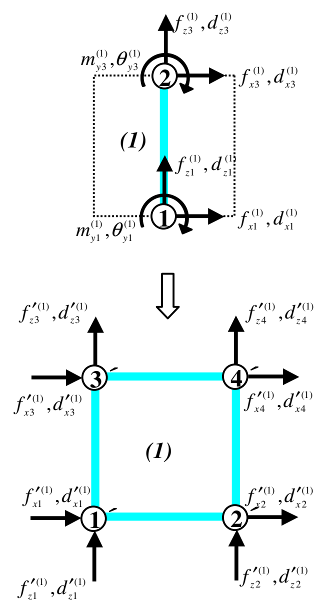

Figure 9 : Line vs. Plate element

Derivation of the member stiffness matrix

The member stiffness matrix is derived by assembling the stiffness matrix of three line elements under the direct stiffness approach based on the nodal force equilibrium condition (Equation (3)).

$$
\begin{Bmatrix} \{\Delta F_1\} \\ \{\Delta F_2\} \\ \{\Delta F_3\} \\ \{\Delta F_4\} \end{Bmatrix} = \begin{bmatrix} [k_{11}^{(1)}] & 0 & [k_{13}^{(1)}] & 0 \\ & [k_{22}^{(2)}] & 0 & [k_{24}^{(2)}] \\ & & [k_{33}^{(1)}]+[k_{33}^{(3)}] & [k_{34}^{(3)}] \\ symm. & & & [k_{11}^{(1)}]+[k_{44}^{(3)}] \end{bmatrix} \cdot \begin{Bmatrix} \{\Delta D_1\} \\ \{\Delta D_2\} \\ \{\Delta D_3\} \\ \{\Delta D_4\} \end{Bmatrix} \quad (3)
$$

The superscripts in parenthesis denote element number and the subscripts are for node number. Expressed using internal (i) and external (e) node notation, Equation (3) becomes

$$\begin{Bmatrix} \{\Delta F_e\} \\ \{\Delta F_i\} \end{Bmatrix} = \begin{bmatrix} [K_{ee}] & [K_{ei}] \\ [K_{ie}] & [K_{ii}] \end{bmatrix} \cdot \begin{Bmatrix} \{\Delta D_e\} \\ \{\Delta D_i\} \end{Bmatrix} \tag{4}$$

On the basis of the assumption that no external force is applied to the internal nodes, Equation (5) is obtained.

$$\{\Delta D_i\} = [K_{ii}]^{-1} \cdot (\{\Delta F_i\} - [K_{ie}]\{\Delta D_e\}), \qquad \{\Delta F_i\} = 0 \tag{5}$$

On substituting Equation (5) into Equation (4), finally, we can obtain the member stiffness matrix in the form of Equation (6), which relates only the external nodal displacements to forces.

$$\{\Delta F_{6\times 1}\} = [K_{6\times 6}]\{\Delta D_{6\times 1}\} \tag{6}$$

$$\text{Where } \begin{array}{l} \{\Delta F_{6\times 1}\} = \{\Delta F_e\} - [K_{ei}] \cdot [K_{ii}]^{-1} \cdot \{\Delta F_i\} \\ [K_{6\times 6}] = ([K_e] - [K_{ei}] \cdot [K_{ii}]^{-1} \cdot [K_{ie}]) \end{array} \tag{7}$$

The stiffness matrix deriving procedure described above is based on the direct stiffness method and the static condensation method, which assembles and reduces the stiffness matrix, respectively.

Plate Element Formulation

Equation (9) shows the relationship between line element and plate element, which have 6 and 8 DOF respectively. The line element can be transformed to plate element based on the two assumptions: one is plane section hypothesis and the other is the stress assumption that transverse stress is zero. The displacement relationship between two elements is, therefore, obtained as Equation (8) and rewritten in the matrix form, Equation (9).

$$\left.\begin{array}{ll} d'^{(1)}_{x1} = d^{(1)}_{x1}, & d'^{(1)}_{z1} = d^{(1)}_{z1} + (D/2) \cdot \theta^{(1)}_{y1} \\ d'^{(1)}_{x2} = d^{(1)}_{x1}, & d'^{(1)}_{z2} = d^{(1)}_{z1} - (D/2) \cdot \theta^{(1)}_{y1} \\ d'^{(1)}_{x3} = d^{(1)}_{x3}, & d'^{(1)}_{z3} = d^{(1)}_{z3} + (D/2) \cdot \theta^{(1)}_{y3} \\ d'^{(1)}_{x4} = d^{(1)}_{x3}, & d'^{(1)}_{z4} = d^{(1)}_{z3} - (D/2) \cdot \theta^{(1)}_{y3} \end{array}\right\} \tag{8}$$

$$\{d'^{(1)}_{8\times 1}\}^T = [T_{8\times 6}] \cdot \{d^{(1)}_{6\times 1}\}^T \tag{9}$$

$$\text{Where } \begin{array}{l} \{d'_{8\times 1}\} = \{d'_{x1}, d'_{z1}, d'_{x2}, d'_{z2}, d'_{x3}, d'_{z3}, d'_{x4}, d'_{z4}\}^T \\ \{d_{6\times 1}\} = \{d_{x1}, d_{z1}, \theta_{y1}, d_{x2}, d_{z2}, \theta_{y2}\}^T \end{array} \tag{10}$$

The plate element is considered as linear plane element with two nodes along an edge and based on the isoparametric formulation which uses the same shape functions to define the element shape as are used to define the displacements within element. A strain-displacement matrix $[B_{3\times 8}]$ and a plane strain-stress relationship are shown in Equation (11) and (12), respectively. The plate nodal displacements in lateral direction transformed from the line element are identical, which makes the transverse incremental strain

$\Delta\varepsilon_x$ become zero in Equation (11). Therefore, the lateral strain cannot be found in an explicit way using Equation (11), but evaluated from Equation (14), which is consistent with the assumption described above.

$$\{\Delta\varepsilon\} = [B_{3\times 8}] \cdot \{\Delta d'_{8\times 1}\} \tag{11}$$

$$\{\Delta\sigma\} = [D]\{\Delta\varepsilon\} \tag{12}$$

$$\text{where} \begin{pmatrix} \{\Delta\varepsilon\} = \{\Delta\varepsilon_x, \Delta\varepsilon_z, \Delta\gamma_{xz}\}^T \\ \{\Delta\sigma\} = \{\Delta\sigma_x, \Delta\sigma_z, \Delta\tau_{xz}\}^T \end{pmatrix}, \quad [D] = [D]_{con.} + [D]_{steel} = \begin{bmatrix} D_{11} & D_{12} & D_{13} \\ D_{21} & D_{22} & D_{23} \\ D_{31} & D_{32} & D_{33} \end{bmatrix} \tag{13}$$

$$\Delta\varepsilon_x = -\frac{D_{12}}{D_{11}} \cdot \Delta\varepsilon_z - \frac{D_{13}}{D_{11}} \cdot \Delta\gamma_{xz} + \frac{\Delta\sigma_x}{D_{11}}, \qquad \Delta\sigma_x = 0 \tag{14}$$

Once the incremental transverse strain is found, complete plane strain components are obtained and then plane stresses can be found. In this study, smeared rotating crack approach is adopted for evaluating stresses and material tangent stiffness matrix from given strains, which is based on averaged stress and strain including the effect of crack and coaxiality between principal strain and principal stress (Vecchio [2], Stevens [3]).

$$[k'_{8\times 8}] = \int [B_{3\times 8}]^T [D][B_{3\times 8}] dV \tag{15}$$

$$\{f'_{8\times 1}\} = \int [B_{3\times 8}]^T \{\sigma\} dV \tag{16}$$

The integrals to obtain the force and stiffness matrix of plate element (Equation (15) and (16)) are numerically evaluated using the two dimensional gaussian quadrature.

Constitutive Model

The plate element is a basic analytical unit in the proposed model. The inelastic properties are determined from the material constitutive laws and therefore the accuracy of the analytical results is, to a great extent, dependent on the material models. The concrete model in principal compressive and tensile direction is shown in Figure. 10, which takes into account the compressive strength softening effect due to tensile strain and the tension stiffening effect, respectively. The compressive strength reduction factor c_1 is

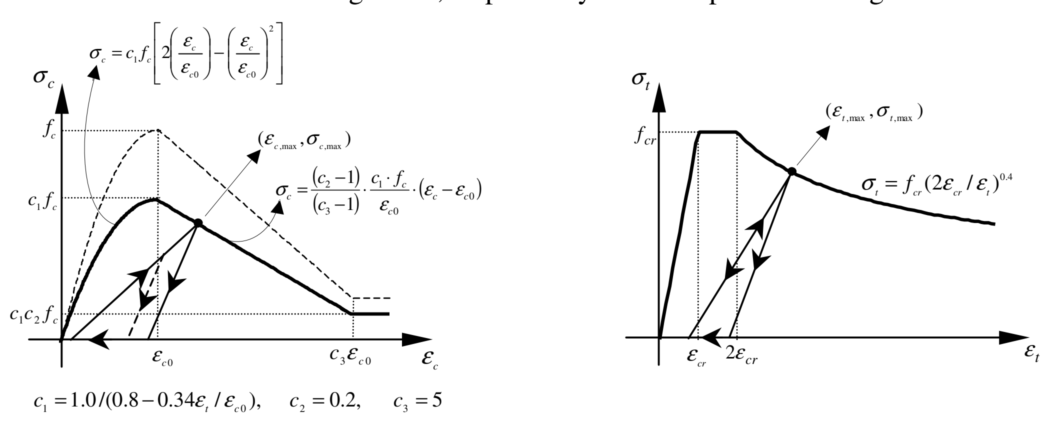

(a) Compression response **(b) tension response**

Figure 10: Constitutive model for concrete

adopted from Vecchio [2] and the descending branch representing the tension stiffening effect is from Isumo [4]. And the reloading and unloading rules under cyclic loading are also presented together with the envelope curve. The constitutive model for both longitudinal and transverse reinforcement used in this study is bi-linear type but incorporating the effect of bond to the concrete. Further details on the reinforcement constitutive model as well as the concrete model can be found in Chen [5].

Iterative Procedure for Numerical Solution

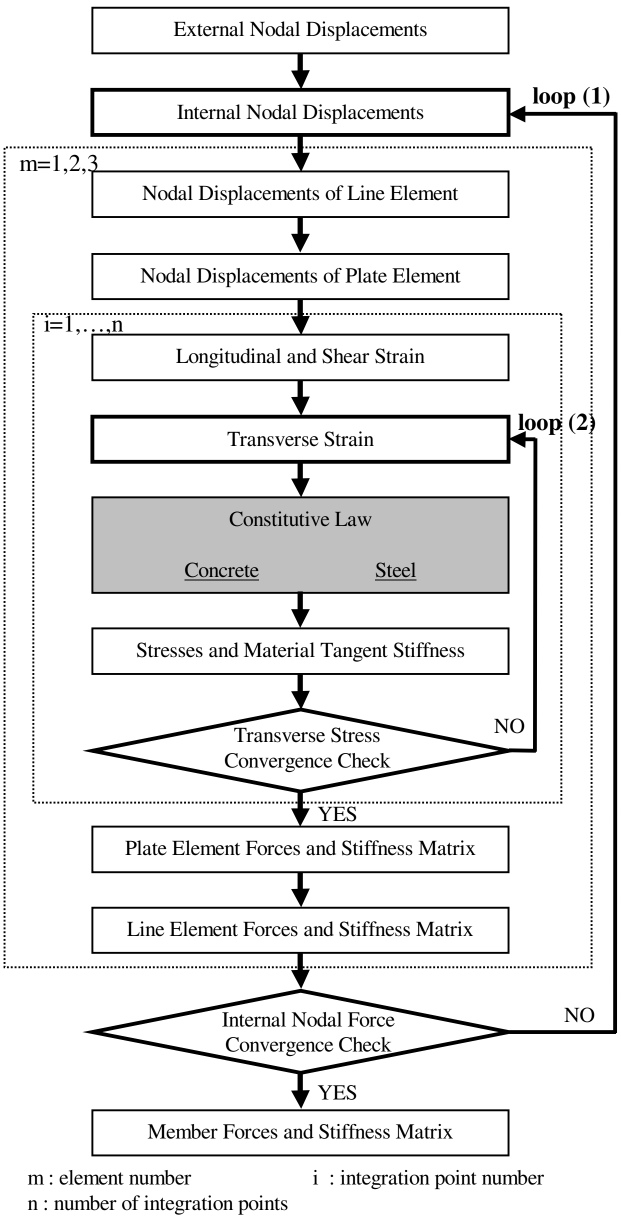

Figure 11: Analysis algorithm for proposed model

A procedure for the nonlinear analysis of the proposed model is summarized in Figure 11, which is established by incorporating the material and element formulation described before. In addition, two iterative schemes imposing internal force equilibrium (Equation (17)) and transverse stress equilibrium (Equation (18)), which resulted from the assumptions made in the proposed element formulation, are introduced in the algorithm. Both of the iterative procedures are continued until the predefined convergence tolerance is satisfied, and the updated material and element stiffness is used for evaluating the residual displacement in the internal nodes (Equation (19)) and the transverse residual strain (Equation (20)), respectively.

$$\{F_i^u\} = \begin{Bmatrix} \{f_3^{(1)}\} + \{f_3^{(3)}\} \\ \{f_4^{(3)}\} + \{f_4^{(2)}\} \end{Bmatrix} (=0) \tag{17}$$

$$\sigma_x^u = \sigma_{cx} + \rho_{sx} \cdot \sigma_{sx} (=0) \tag{18}$$

$$\{\Delta D_i\} = [K_{ii}]^{-1} \cdot \{F_i^u\} \tag{19}$$

$$\Delta\varepsilon_x = -\sigma_x^u / D_{11} \tag{20}$$

However, the displacements assigned at external nodes should not be changed in the iteration loop (1), as the displacement compatible condition at the external nodes should be insured. In the same manner, explicitly calculated strains (i.e. longitudinal and shear strain) are not updated also in the iteration loop (2), in which only the lateral strains at each integration point are computed using renewed material stiffness and residual stress obtained by imposing the equilibrium between transverse steel stress and concrete stress (Equation (18)). In particular, initial values for the internal displacements $\{\Delta D_i\}$ and transverse strain $\Delta\varepsilon_x$ can be found according to the Equation (5) and Equation (14), respectively, which correspond to the Equation (19) and (20) after initialization.

ANALYSIS AND RESULTS

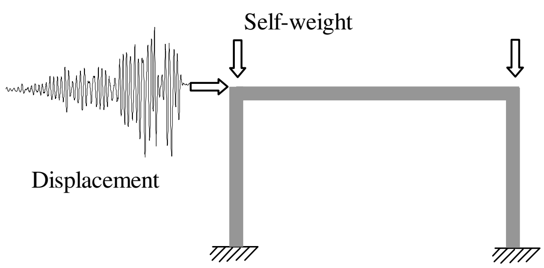

Figure 12 : plane frame subtracted from specimen

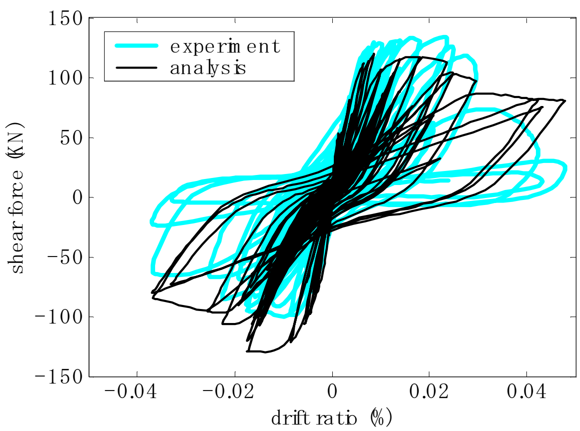

Figure 13 : force vs. drift-ratio

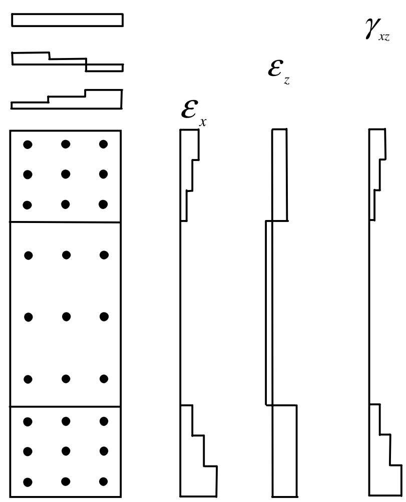

Figure 14 : strain distribution

For the experimental results from TOH12.5 to JMA50 where little strength deterioration was occurred, three-dimensional dynamic analysis has already been performed with two analytical models such as classical fiber model and lumped plasticity model (i.e. one-component model) in Kim [6]. The fiber model showed a better correlation between the calculated and the observed data rather than one-component model. This is mainly because the axial-bending and the biaxial bending interaction were introduced in the former, but not in the latter. Both of the models, however, failed to simulate the post-peak response during CHI50 input.

As noted previously, the proposed model is available only in the two-dimensional problem at current stage. However, the test specimen experienced torsional response under three-dimensional effect despite unidirectional seismic load was applied, and therefore it is beyond the scope of this model to simulate the experimental results.

As the alternative to the three-dimensional dynamic analysis of the specimen, two-dimensional static analysis is performed on a weak frame depicted in Figure1. Obviously, this could be the source of error and the model might not be suitable for and even incapable of simulating the 3-D experimental results since so many characteristics affecting the experimental results are ignored and not included in analytical procedure. Nonetheless, this analytical study has the meaning in terms of proving the stability in iterating nonlinear numerical solution and the capability of incorporating the strength degradation effects. Thus, the displacement controlled static analysis was performed with the application of the lateral displacement record at the 1st story, while the constant compression axial load corresponding to the self-weight was maintained (Figure.12). Taking into account the residual deformation and the stiffness degrading effect observed in the experimental results at the end of each input, the frame was subjected to the displacement record connected from TOH12.5 to CHI50 in succession.

Figure.13 shows the calculated force-drift ratio relationship together with the observed one. Although the analytical model did not provide a satisfactory accuracy in predicting the maximum shear strength, the model adequately represented the strength deterioration feature. The difference of strength deteriorating rate between the model and the experimental data might be attributed to the variable axial load accelerating the strength degradation in experimental case, while it was not considered in analytical one. In addition, biaxial effect might also be associated with rapidly degrading strength observed in the experimental results.

Using the strain values such as transverse, longitudinal and shear strain calculated at integration points, each strain distribution is illustrated in Figure.14. It should be noted that the level of the strains developed in the mid-height region were significantly low compared to those of hinge regions and remained within elastic range throughout the whole response, and the shear strain distribution is constant along the section, as a consequence of the stress assumption made in the element formulation. Although these features resulting from the proposed element formulation are inevitable and could be apparent limitations in further realistic evaluation of inelastic behaviour of RC columns, these effects on the analytical results would not be so significant in most cases that they may be disregarded.

CONCLUSIONS

Based on the results of the experimental and the analytical investigation presented herein, the following conclusions can be drawn.

Throughout all the loading stages from elastic to inelastic range, the lateral displacement responses of the column side (weak or flexible frame) were much lager than those of the wall side (strong or stiff frame), which was expected and attributed to the considerable stiffness and strength eccentricity. In particular, the torsional response was a little lager in inelastic responses than in elastic, which may be due to the large strength eccentricity.

The collapse process of reinforced concrete columns during CHI50 input, shear strength deterioration resulting in axial load failure along with inelastic load reversals, was interpreted with the detailed local responses, such as transverse steel strain, lateral and vertical displacements, shear and axial forces and their relationships.

An analytical member model of column in frame analysis is proposed based on stress-strain relation formulated from the material constitutive model. Static analysis of the test specimen was carried out using the new model, where the stress and force equilibrium condition obtained from the dynamic test was applied with numerical iterative procedure. A fair correlation was obtained between the test and analysis. The model may be used to incorporate the bending, shear and axial force interaction and the strength deterioration under the cyclic loading.

The proposed model is limited to two-dimensional analysis and needs to be extended to three-dimensional model simulating including as confinement effect and multi-axial interaction. The material constitutive law should also be verified further to improve the accuracy of the analytical model.

REFERENCES

1. Kim Y, Kabeyasawa T. “Shaking Table Test of Reinforced Concrete Frames with/without Strengthening for Eccentric Soft First Story.” Proceedings of the Fourth US-Japan Workshop on

Performance-Based Earthquake Engineering Methodology for Reinforced Concrete Building Structures, Toba, Japan, pp.119-134, 2002
2. Vecchio F, Collins MP. “Modified Compression Field Theory for Reinforced Concrete Elements Subjected to Shear.” ACI Journal, Proceedings 1986; 83(2) : pp.219- 231
3. Stevens NJ, Uzumeri SM, Collins MP. “Reinforced Concrete Subjected to Reversed Cyclic Shear – Experiments and Constitutive Model.” ACI Structural Journal 1991; 88(2) : pp.135-146
4. Izumo J, Shima H, Okamura H. “Analytical Model for RC Panel Elements Subjected to In-plane forces.” Concrete Library International, JSCE 1989, No.12 : pp.155-181.
5. Chen S, Kabeyasawa T. "Modeling of reinforced concrete shear wall for nonlinear analysis." Paper No. 1596, Proceedings of the 12th World Conference on Earthquake Engineering, CD-ROM, New Zealand, January 2000, 8pp.
6. Kim Y, Kabeyasawa T. “Nonlinear earthquake response analysis on eccentric piloti reinforced concrete structure.” Summaries of Technical Papers of Annual Meeting Architectural Institute of Japan, pp.907-908, 2003 (in Japanese)